β-delayed neutron emissions from $N > 50$ gallium isotopes

R. Yokoyama,[1,2,*] R. Grzywacz,[1,3] B. C. Rasco,[3,1] N. Brewer,[3,1] K. P. Rykaczewski,[3] I. Dillmann,[4] J. L. Tain,[5] S. Nishimura,[6] D. S. Ahn,[6] A. Algora,[5,7] J. M. Allmond,[3] J. Agramunt,[5] H. Baba,[6] S. Bae,[8] C. G. Bruno,[9] R. Caballero-Folch,[4] F. Calvino,[10] P. J. Coleman-Smith,[11] G. Cortes,[10] T. Davinson,[9] C. Domingo-Pardo,[5] A. Estrade,[12] N. Fukuda,[6] S. Go,[6] C. J. Griffin,[9] J. Ha,[8,6] O. Hall,[9] L. J. Harkness-Brennan,[13] J. Heideman,[1] T. Isobe,[6] D. Kahl,[9] M. Karny,[14] T. Kawano,[15] L. H. Khiem,[16] T. T. King,[1] G. G. Kiss,[6,7] A. Korgul,[14] S. Kubono,[6] M. Labiche,[11] I. Lazarus,[11] J. Liang,[17] J. Liu,[18,6] G. Lorusso,[19,20,6] M. Madurga,[1] K. Matsui,[6,21] K. Miernik,[14] F. Montes,[22] A. I. Morales,[5] P. Morrall,[11] N. Nepal,[12] R. D. Page,[13] V. H. Phong,[6,23] M. Piersa-Siłkowska,[14] M. Prydderch,[24] V. F. E. Pucknell,[11] M. M. Rajabali,[25] B. Rubio,[5] Y. Saito,[4] H. Sakurai,[6] Y. Shimizu,[6] J. Simpson,[11] M. Singh,[1] D. W. Stracener,[3] T. Sumikama,[6] H. Suzuki,[6] H. Takeda,[6] A. Tarifeño-Saldivia,[10] S. L. Thomas,[24] A. Tolosa-Delgado,[5] M. Wolińska-Cichocka,[26] P. J. Woods,[9] and X. X. Xu[18]

[1]*Department of Physics and Astronomy, University of Tennessee, Knoxville, Tennessee 37996, USA*
[2]*Center for Nuclear Study, the University of Tokyo, 2-1 Hirosawa, Wako, Saitama 351-0198, Japan*
[3]*Physics Division, Oak Ridge National Laboratory, Oak Ridge, Tennessee 37830, USA*
[4]*TRIUMF, Vancouver, British Columbia V6T 2A3, Canada*
[5]*Instituto de Fisica Corpuscular (CSIC-Universitat de Valencia), E-46071 Valencia, Spain*
[6]*RIKEN, Nishina Center, 2-1 Hirosawa, Wako, Saitama 351-0198, Japan*
[7]*MTA Atomki, Bem ter 18/c, Debrecen H4032, Hungary*
[8]*Department of Physics and Astronomy, Seoul National University, 1 Gwanak-ro, Gwanak-gu, Seoul 08826, Republic of Korea*
[9]*School of Physics and Astronomy, University of Edinburgh, EH9 3FD Edinburgh, United Kingdom*
[10]*Universitat Politècnica de Catalunya (UPC), E-08028 Barcelona, Spain*
[11]*STFC Daresbury Laboratory, Daresbury, Warrington WA4 4AD, United Kingdom*
[12]*Department of Physics and Science of Advanced Materials Program, Central Michigan University, Mount Pleasant, Michigan 48859, USA*
[13]*Department of Physics, University of Liverpool, Liverpool L69 7ZE, United Kingdom*
[14]*Faculty of Physics, University of Warsaw,PL-02-093 Warsaw, Poland*
[15]*Los Alamos National Laboratory, Los Alamos, New Mexico 87545, USA*
[16]*Institute of Physics, Vietnam Academy of Science and Technology, 10 Dao Tan, Ba Dinh, Hanoi, Vietnam*
[17]*Department of Physics and Astronomy, McMaster University, Hamilton, Ontario L8S 4M1, Canada*
[18]*Department of Physics, University of Hong Kong, Pokfulam Road, Hong Kong*
[19]*National Physical Laboratory (NPL), Teddington, Middlesex TW11 0LW, United Kingdom*
[20]*Department of Physics, University of Surrey, Guildford, GU2 7XH, United Kingdom*
[21]*Department of Physics, University of Tokyo, 7-3-1 Hongo, Bunkyo-ku, Tokyo 113-0033, Japan*
[22]*National Superconducting Cyclotron Laboratory, Michigan State University, East Lansing, Michigan 48824, USA*
[23]*University of Science, Vietnam National University, Hanoi 120062, Vietnam*
[24]*STFC Rutherford Appleton Laboratory, Harwell Campus, Didcot OX11 0QX, United Kingdom*
[25]*Department of Physics, Tennessee Technological University, Cookeville, Tennessee 38505, USA*
[26]*Heavy Ion Laboratory, University of Warsaw, Warsaw PL-02-093, Poland*

(Received 19 July 2023; accepted 7 November 2023; published 8 December 2023)

β-delayed γ-neutron spectroscopy has been performed on the decay of $A = 84$ to 87 gallium isotopes at the RI-beam Factory at the RIKEN Nishina Center using a high-efficiency array of ^{3}He neutron counters (BRIKEN). β-$2n$-γ events were measured in the decays of all of the four isotopes for the first time, which is direct evidence for populating the excited states of two-neutron daughter nuclei. Detailed decay schemes with the γ branching ratios were obtained for these isotopes, and the neutron emission probabilities (P_{xn}) were updated from the previous study. Hauser-Feshbach statistical model calculations were performed to understand the experimental branching ratios. We found that the P_{1n} and P_{2n} values are sensitive to the nuclear level densities of $1n$ daughter nuclei and showed that the statistical model reproduced the P_{2n}/P_{1n} ratio better when experimental levels plus shell-model level densities fit by the Gilbert-Cameron formula were used as the level-density input. We also showed the neutron and γ branching ratios are sensitive to the ground-state spin of the parent nucleus. Our statistical model analysis suggested $J \leqslant 3$ for the unknown ground-state spin of the odd-odd nucleus ^{86}Ga, from the $I_\gamma(4^+ \rightarrow 2^+)/I_\gamma(2^+ \rightarrow 0^+)$ ratio of ^{84}Ga and the P_{2n}/P_{1n} ratio. These results show the necessity of detailed

*yokoyama@cns.s.u-tokyo.ac.jp

 ©2023 American Physical Society

understanding of the decay scheme, including data from neutron spectroscopy, in addition to γ measurements of the multineutron emitters.

DOI: 10.1103/PhysRevC.108.064307

I. INTRODUCTION

β-delayed neutron emission is a decay mode found in very neutron-rich nuclei where the energy window of the β decay (Q_β) is high enough to populate excited states of the daughter nucleus above neutron separation energy (S_n). This process was first observed in 1939 [1], and there have been 300 one-neutron emitters found [2,3]. Moving further away from the line of stability to more neutron-rich nuclei, Q_β increases rapidly and neutron separation energies continue to decrease, which makes delayed multineutron emission energetically available.

The number of neutrons emitted in decays of neutron-rich nuclei is an important input for astrophysical r-process abundance calculations. It affects the final isobaric abundance pattern by providing neutrons for the late-time captures process and changing the decay path back to stability [4]. Until recently, the neutron emission probabilities for the r-process abundance calculations relied on predictions based on the simplified assumption that only x-neutron emission will occur when β decay fed a state above S_{xn}, and the effects of less-than-x-neutron channels are negligible. We call this simplified approach the "cutoff" model. In this model, the neutron emission probabilities are proportional to the integrated population of states in the available energy window, $Q_\beta - S_{(x+1)n} < E_\beta < Q_\beta - S_n$, and are directly related to the β-decay strength function. This model was used in many theoretical calculations of P_{xn} values, for example, the global calculations by Möller *et al.* [5], Marketin [6], or recently by Minato *et al.* [7]. In this approach, a strong dependence of delayed neutron emission on the decay strength distribution within a specific energy window is observed, leading to predictions of very strong multineutron emission channels for most exotic isotopes. However, this assumption may oversimplify the reality, and competition between multineutron emission channels should be considered. By assuming sequential emissions of neutrons from a state above S_{2n} in the daughter nucleus, the final number of neutrons emitted in the the sequence depends on whether or not the first neutron took more energy than $S_{2n} - S_{1n}$. If the first emission populated a state below S_{1n}, two-neutron emission is no longer possible. Therefore, such competition could reduce multineutron emission probabilities from those predicted by the cutoff model assumption.

For nuclei with $Q_\beta < S_{2n}$, γ emission from neutron-unbound states is the only competition that can reduce the neutron emission probability. The neutron-γ competition was previously considered by experimentalists and theorists [8–12]. The significance of the relative competition between multineutron emission channels in the $Q_\beta > S_{2n}$ nuclei was quantitatively discussed in the theoretical work by Mumpower *et al.* [13] and a modified global prediction for neutron emission probabilities was provided using the QRPA strength distribution [14]. It was concluded that relative neutron emission branching ratios can affect the results of r-process nucleosynthesis models. However, the experimental data, which enable the evaluation of the competition between multi-neutron emission channels for the r-process nuclei, are almost nonexistent. According to Ref. [2], there are only a few two-neutron emitters, and no three-or-more-neutron emitters are known so far in nuclei with $Z > 26$, which are relevant for r-process modeling.

β-delayed two-neutron ($2n$) emission was first observed in 1979 [15] in ^{11}Li. Unlike for one-neutron emitters, two-neutron emission probabilities (P_{2n}) have been measured for fewer than ten nuclei heavier than iron. This is due to the challenges of producing sufficiently neutron-rich nuclei. Most identified $2n$ emitters are nuclei lighter than iron from Li to K [16–20]. For nuclei heavier than iron, there are known $2n$ emitters in ^{98}Rb [21], ^{100}Rb [22], and ^{136}Sb [23] with small branching ratios of 0.060(9)%, 0.16(8)%, and 0.14(3)%, respectively. The first observation of strong two-neutron emission in the region relevant to the r process was achieved for ^{86}Ga with $P_{2n} = 20(10)\%$ by Miernik *et al.* [24]. Other than that, the existence of a decaying branch to the two-neutron-emission daughter nuclei is confirmed by β-γ spectroscopy without a neutron measurement in some nuclei, such as ^{140}Sb [25] or ^{134}In decay [26].

With the advent of radioactive ion beam facilities and efficient neutron detectors [27–30], β-delayed multi-neutron emitters are becoming accessible for study, and a number of papers on the new two-neutron measurements have recently been published [31–33]. The $N > 50$ Ga isotopes are some of the best candidates to study multineutron emission in nuclei heavier than iron since they are known to have strong neutron-emission branching ratios. This is due to their large energy window for β decay where most of the Gamow-Teller strength B(GT) is concentrated above neutron separation energies because of the $N = 50$ shell gap [34]. Large P_{1n} values were measured for Ga isotopes, in $^{83–86}$Ga [24,34–37].

In this work, we have measured the β decays of $^{84–87}$Ga. P_{1n} and P_{2n} values of these isotopes were reported previously in a Rapid Communication [31]. We have found large P_{1n} values and unexpectedly small P_{2n} values even for those Ga isotopes where the major part of the B(GT) is expected to be concentrated above S_{2n}. This was interpreted as a signature of one-neutron emission from two-neutron unbound states. These results confirmed experimentally for the first time that the assumption of the cutoff model is not valid when the two-neutron emission channel is energetically available, and the competition between $2n$ and $1n$ emission processes has to be considered [31].

The β-delayed neutron emission is a two-step process, where the β-decay strength distribution determines the first stage. In the second stage one has to consider the neutron-emission probability from excited nuclear states in β-decay daughter. The key questions for the modeling of the

second phase of this process are the degree to which the nuclear structure affects neutron emission and how the details of this process should be modeled.

The work by Mumpower *et al.* [13] implements the strength function using the quasiparticle random-phase approximation and the Hauser-Feshbach statistical model (QRPA-HF) for particle and γ-ray emissions [38]. This model calculates P_{1n} or P_{2n} by following statistical decays of both the delayed-γ and neutron emission one by one until all the excitation energy is exhausted. The authors of Ref. [13] explored this framework and found only a slight improvement in branching ratios near stability but a substantial difference for neutron-rich nuclei closer to the drip line. This is due to the dominance of the multineutron emission processes in the very exotic nuclei that are typically involved in the *r* process. The statistical model was then applied to the global calculation by Möller *et al.* [14], and the new P_{xn} predictions are in better agreement with our experimental data [31] compared to the ones using the cutoff model [5].

In this paper, we show a more detailed analysis of the P_{xn} values to narrow down the uncertainties that originated from the energy-dependent efficiency of the neutron detector and updated results from the previous paper, together with the new results from the γ-ray analysis. We also report a detailed analysis of the statistical model calculations using more realistic level densities from our experimental data and shell-model calculations, combined to discuss the sensitivity of the branching ratios to the nuclear structure in β-delayed neutron emission models.

II. EXPERIMENTAL DETAILS

Neutron-rich Ga ($Z = 31$) isotopes were studied by means of β-neutron-γ spectroscopy at the RI Beam Factory (RIBF) of the RIKEN Nishina Center. The neutron-rich nuclei were produced by in-flight fission of a 345-MeV/nucleon $^{238}U^{86+}$ beam on a 4-mm-thick ^{9}Be production target. The measurements were performed in two independent runs with a slight $B\rho$ (magnetic rigidity) difference. We call these runs run #1 and #2 in this paper. The typical intensities of the primary ^{238}U beam were ≈ 40 and ≈ 60 p nA for runs #1 and #2, respectively. Fission fragments were separated and identified in the BigRIPS in-flight separator [39] on an event-by-event basis by their proton numbers (Z) and the mass-to-charge ratio (A/Q). These quantities were obtained by measuring $B\rho$, the time of flight (TOF), and energy loss (ΔE) in BigRIPS. The TOF was obtained from the time difference between plastic scintillation counters at the achromatic foci F3 and F7. The $B\rho$ values were obtained by ion trajectory reconstruction using position and angular information measured by position-sensitive parallel-plate avalanche counters (PPACs) [40]. The atomic number was obtained by measuring the energy loss (ΔE) in an ionization chamber [41] at the F7 focal plane. A detailed explanation of the particle identification at BigRIPS is found in Ref. [42,43]. The particle identification plot is shown in Fig. 1. There were 9×10^6, 3×10^6, 7×10^4, and 6×10^3 $^{84-87}$Ga ions implanted in total in the two runs, respectively.

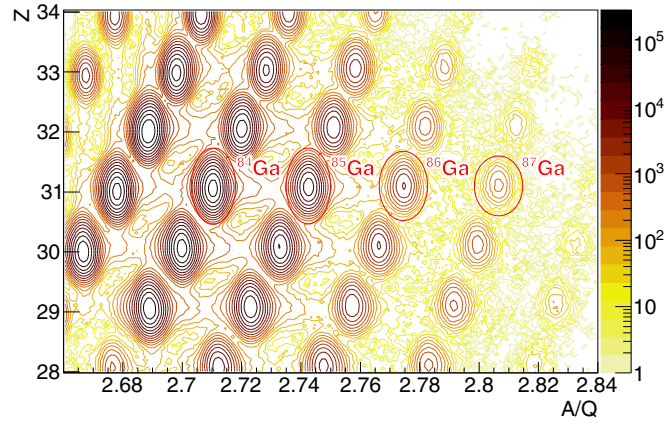

FIG. 1. Particle identification plot of the secondary beam at BigRIPS. The red ellipses indicate the gates applied to select each Ga ion. This plot shows the sum of the two different runs (see the text).

The secondary beam was transported to the F11 focal plane and implanted into active stoppers made of double-sided silicon-strip detectors (DSSDs) for ion and β correlation. The AIDA (Advanced Implantation Detector Array) [44] was used in the run #1 whereas WAS3ABi [45] was employed for the run #2. A YSO scintillation detector [46] was also installed as a stopper for lighter mass ions than Ni. AIDA is a stack of six layers of DSSDs whose wafers have a thickness of 1 mm and is segmented into 128 strips with 0.560 mm pitch in both x and y directions. β particles detected within a 1.96-mm (3.5 strip width) radius of an implanted ion were correlated. WAS3ABi has four layers of DSSDs with 16 3-mm strips for x and y. The ion-β correlation was made by a 3-mm (1 strip width) distance. The typical rate of the ion implantation in AIDA during the run #1 was $\approx$150 cps in total, whereas that in WAS3ABi during the run #2 was $\approx$60 cps. Among all the ions implanted in the DSSD arrays, about 18% were ^{84}Ga.

The active stopper detector was placed in the center of a high-density polyethylene moderator of BRIKEN [30,48,49]. The BRIKEN system is composed of 140 proportional counters filled with ^{3}He gas for neutron detection and two clover-type high-purity Ge detectors from the CLARION array of Oak Ridge National Laboratory [50] for high-resolution γ-ray detection. In this configuration, BRIKEN has 62(2)% neutron efficiency (ϵ_n) at $\approx$1 MeV neutron energy [30].

The photopeak efficiency of the two clover detectors for 1 MeV γ rays is $\approx$3.5% for a point source at the center of the array. Since the implantation distribution in each layer of the detectors is different for each nuclide, Monte Carlo simulations by GEANT4 were performed to estimate nuclide-by-nuclide efficiencies using the experimental implantation profiles. The systematic error in the efficiencies from the geometrical uncertainties in the experimental setup was estimated as 4% by changing the clover position in the simulation by 2 mm, which is the maximum uncertainty expected from the geometrical precision of the detector setup. The γ-ray intensities in the decay of ^{77}Ni and ^{85}Ga are compared with previous studies [36,47] as shown in Fig. 2. Our γ-intensity analysis

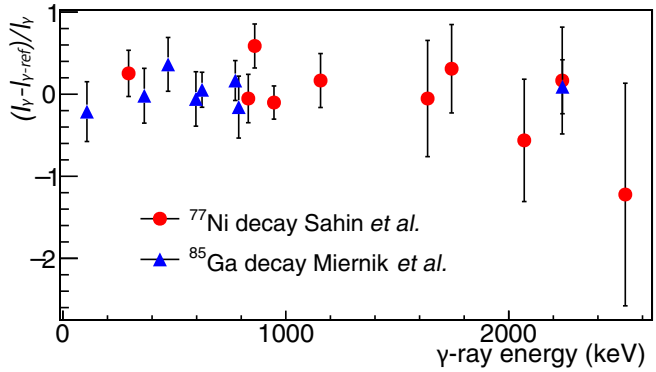

FIG. 2. Comparison of the γ-ray intensities between this work (I_γ) and previous studies ($I_{\gamma\text{-ref}}$). The red circle shows the γ rays in the decay of ^{77}Cu previously reported by Sahin *et al.* [47] and the blue triangles are the ones from ^{85}Ga decay by Miernik *et al.* [36].

is consistent with previous work in the energy range of ≈100 keV and ≈2 MeV.

III. RESULTS

A. P_{xn} Values

The neutron-gated ion-β time spectra for ^{84}Ga and ^{85}Ga decays obtained in run #2 are presented in Fig. 3. The same plots for ^{86}Ga and ^{87}Ga were shown in the previous publication [31]. Neutron events were correlated with a β-decay event if it was in a 200-μs time window after the β-ray emission. The half-lives ($T_{1/2}$) and initial decay rates at $T_\beta - T_{\rm ion} = 0$ for each neutron multiplicity (A_{0n}, A_{1n}, and A_{2n}) were obtained by binned maximum likelihood fitting to a function with the decays of parent, daughter, 1n daughter, and 2n daughter, as well as a linear background. The half-lives of the daughter nuclei, ^{84}Ge and ^{85}Ge, were fixed to the literature values 942 and 494 ms, respectively [51]. Short fitting ranges from 6 ms to 510 ms for ^{84}Ga and 550 ms for ^{85}Ga ($\approx 6 \times T_{1/2}$) were employed in order to minimize uncertainty coming from descendant decays. In the 1n and 2n spectra, the portion of the parent decay is larger than those of 0n decays because the descendant nuclei are less exotic and have lower P_n values. Half-lives of 1n spectra are chosen as the reported values since the 1n spectra had a smaller component from descendant nuclei than 0n spectra and higher statistics than those of 2n decays.

In the fitting of 0n and 2n spectra, the half-lives of parent nuclei were fixed to the values obtained from 1n spectra. Since the neutron efficiency is not 100%, A_{0n} includes 1n or 2n events with undetected neutrons. Also, A_{1n} and A_{2n} includes 0n or 1n events in coincidence with random background neutrons. A conversion matrix E from P_{xn} to A_{xn} is defined as

$$\begin{pmatrix} A_{0n} \\ A_{1n} \\ A_{2n} \end{pmatrix} = E \begin{pmatrix} P_{0n} \\ P_{1n} \\ P_{2n} \end{pmatrix}, \tag{1}$$

as shown in Ref. [49]. The P_{xn} values are derived from A_{xn} values by calculating the inverse matrix, E^{-1}. The random neutron coincidence probabilities, r_{xn}, in the matrix shown as Eq. (2) of Ref. [49], were estimated from the spectra of nuclei with $Q_\beta < S_{2n}$. The probabilities of having one background neutron in the 200-μs correlation time window over those for no neutron are estimated to be $r_{1n}/r_{0n} = 0.010$ and 0.012 for runs #1 and #2, respectively. We assumed that the random neutrons are independent of each other, providing the relationship $r_{2n} = r_{1n}^2$. The half-lives and branching ratios were obtained separately for each of the two runs since the r_{1n} values are slightly different due to the beam rate, degrader thickness, and implant detector setups. The $T_{1/2}$ and P_{xn} values obtained for each run, and the average of the two, are summarized in

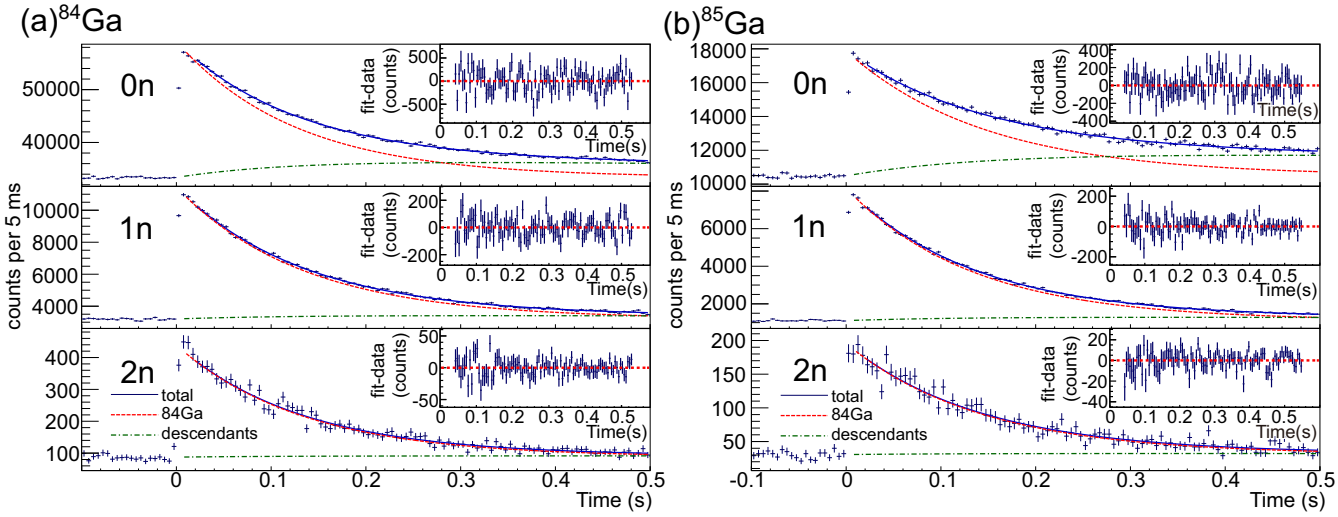

FIG. 3. The decay curves gated by neutron multiplicity 0, 1, and 2 for (a) ^{84}Ga and (b) ^{85}Ga. The solid blue curves represent the fitting functions. The dashed red curves show the decay components of the precursor nuclei. The dashed-dotted green curves are the sums of the daughter decays, including neutron emission branches. The plots at the top right corners of each spectrum are the residuals of the decay spectra from the fitting function.

TABLE I. Half-lives, P_{1n}, and P_{2n} obtained in this study. Values from the two different runs and their weighted averages (adop.) are shown.

		Branching ratio (%)	
Nuclide	$T_{1/2}$ (ms)	P_{1n}	P_{2n}
^{84}Ga run#1	95.0(25)	38.2(21)[a]	1.91(17)[a]
^{84}Ga run#2	97.6(12)	37.0(4)[a]	1.87(7)[a]
^{84}Ga adop.	97.1(11)	37.0(4)[a](11)[b]	1.88(6)[a](11)[b]
^{85}Ga run#1	101(4)	73(4)[a]	1.8(3)[a]
^{85}Ga run#2	95.3(10)	76.4(18)[a]	1.53(14)[a]
^{85}Ga adop.	95.6(10)	75.8(18)[a](24)[b]	1.58(13)[a](9)[b]
^{86}Ga run#1	53(4)	57(6)[a]	17.8(22)[a]
^{86}Ga run#2	51(2)	59.9(23)[a]	14.1(10)[a]
^{86}Ga adop.	51(2)	59.5(21)[a](18)[b]	14.7(9)[a](11)[b]
^{87}Ga run#1	31(9)	73(31)[a]	18(18)[a]
^{87}Ga run#2	24(8)	72(9)[a]	8.5(28)[a]
^{87}Ga adop.	27(6)	72(9)[a](2)[b]	8.7(28)[a](5)[b]

[a]Statistical errors.
[b]Systematic errors.

Table I. Details of the general analysis for obtaining P_{xn} values are described in [49].

Although the BRIKEN array has minimized energy dependency of the neutron detection efficiency up to a few MeV, the efficiency still drops at a few MeV or higher, due to its large high-density polyethylene moderator. The neutron efficiency varies from 50% for 5 MeV to 68% for low-energy neutrons, as shown in the yellow dashed curve in Fig. 4, and therefore we need to make an assumption about the neutron spectrum unless it is measured experimentally. In the previous paper [31], we reported P_{xn} values with larger uncertainties by using shell-model-generated neutron spectra. These spectra provide a lower limit on the neutron efficiency since it assumes that all the excitation energies are taken out by neutrons but not by γ rays. In the current work, we applied the statistical model calculation described later in Sec. IV to narrow down the neutron efficiency by convoluting the calculated energy spectra and the simulated efficiency curve as shown in Fig. 4.

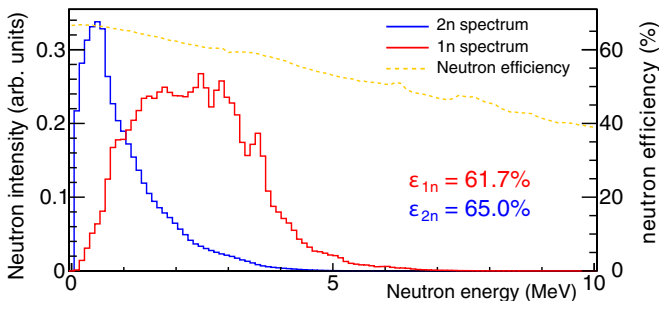

FIG. 4. Neutron energy spectra expected in the decay of ^{86}Ga predicted from the statistical model calculation using B(GT) predicted by the shell model [34]. The red and blue histograms show the single-neutron energy spectra for 1n and 2n channels, respectively. The dashed orange curve shows the simulated neutron detection efficiency of the BRIKEN array [30] whose axis is on the right-hand side of the plot.

For the systematic errors, the neutron efficiencies were varied by shifting the GT strength 500 keV in the statistical model calculations. The P_{xn} values are reported in Table I. The obtained values have smaller systematic errors than those reported in the previous paper [31]. The dataset of run #1 was analyzed before, and the P_{xn} and $T_{1/2}$ values are summarized in [52]. There are minor differences between values presented in those previous works and this paper owing to updated neutron efficiency analysis.

B. n-β-γ Analysis

In the following subsections, β-neutron gated γ spectra for the decay of $^{84-87}$Ga are shown. The γ rays following β decays were correlated with a 7-μs time window. The γ-ray intensities per precursor decay (I_γ) are deduced from the γ-ray peak area and the number of β events (N_β) that were used to generate the γ-ray spectrum. I_γ is defined as

$$I_\gamma = A_{\rm peak}/(\varepsilon_\gamma \varepsilon_{xn} N_\beta), \tag{2}$$

where ε_γ and ε_{xn} are the γ-ray and x-neutron detection efficiencies by simulations. N_β is the integral of the positive part of the time spectrum up to the time window (t_w), subtracted by the negative part as a random β-implant correlations:

$$N_\beta = r_{\rm precursor}\left(\int_0^{t_w} N_{\rm tot}(t)dt - \int_{-t_w}^{0} N_{\rm tot}(t)dt\right). \tag{3}$$

Ratio of the precursor activity in the total Bateman function ($r_{\rm precursor}$) is calculated as follows:

$$\begin{aligned} r_{\rm precursor} &= \frac{A_0}{A_0 + A_1 + \cdots}, \\ A_0 &= \int_0^{t_w} e^{-\lambda_0 t} dt, \\ A_1 &= \int_0^{t_w} \frac{\lambda_1}{\lambda_1 - \lambda_0}(e^{-\lambda_0 t} - e^{-\lambda_1 t})dt. \end{aligned} \tag{4}$$

$A_0, A_1, \ldots$ and $\lambda_0, \lambda_1, \ldots$ are the activities and decay rates of precursor (0) and descendant (1, 2, …) nuclides.

1. ^{84}Ga

Delayed-neutron emission in the decay of ^{84}Ga was previously measured by using proton-induced fission of ^{238}U at HRIBF, ORNL [35] and by photofission of uranium targets at ALTO, IPN Orsay [37,53] and at ISOLDE, CERN[34]. The reported P_{1n} values by those previous works are 74(14)% [54], 53(20)% [37], and 40(7)% [34], respectively. The adopted value from this work is 37.0(12)%, which supports the last two values. The adopted half-life of ^{84}Ga from this work, 97.1(11) ms, is consistent with the value reported before, 85(10) ms [55].

Figure 5 shows the γ-ray energy spectra in the decay of ^{84}Ga gated by the neutron multiplicities. There is a clear peak at 1348 keV in the 2n gated spectrum in the figure which is interpreted as $2^+ \rightarrow 0^+$ of ^{82}Ga in the β_{2n} branch. In the previous work [37], there is a candidate at this energy in the $\beta - n$ gated γ spectrum with very limited statistics. The γ-ray energies and intensities measured in this work are summarized in Table II.

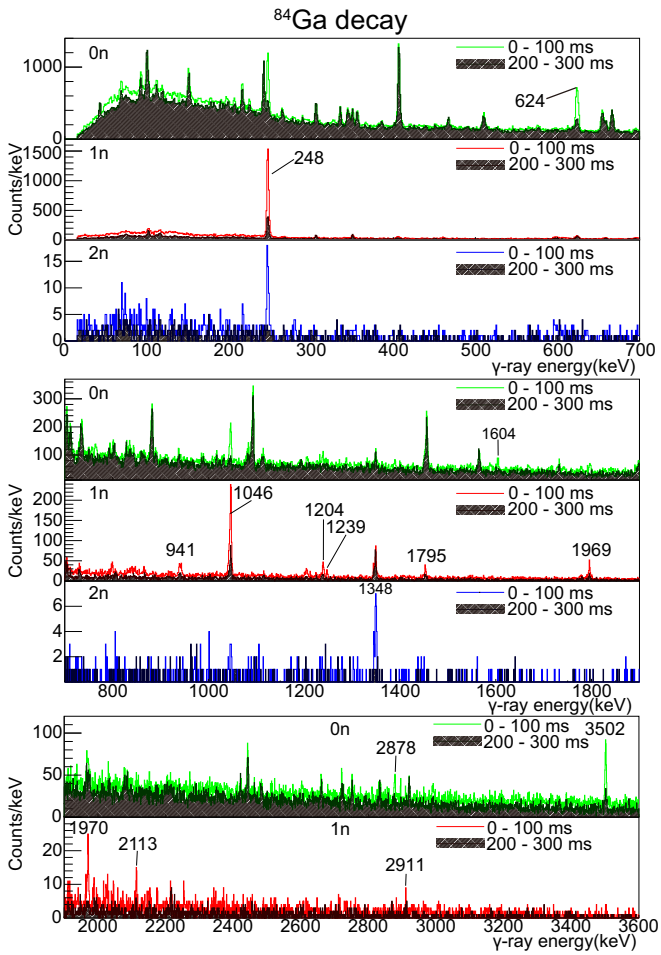

FIG. 5. γ-ray energy spectra of ^{84}Ga gated by neutron multiplicities. Green, red, and blue histograms show γ rays observed with the neutron multiplicity equal to 0, 1, and 2, respectively. Histograms with a time window from 0 to 100 ms are drawn in lighter colors while the ones from 200 to 300 ms are drawn in darker colors and hatched in order to distinguish if the peaks originate in the parent ^{84}Ga decay or from the decay of the descendant nuclei. Peaks that are distinct only in the lighter colors are regarded as the γ rays from the decay of ^{84}Ga.

Figure 6 shows the decay scheme of ^{84}Ga obtained in this work. This scheme is consistent with the reported one [53] except for the 2113-keV line, which has not been reported in the literature.

2. ^{85}Ga

The β-γ spectrum of ^{85}Ga was previously measured by Korgul *et al.* [59] and then by Miernik *et al.* [36] including the β-n-γ spectrum. We observed the β-n-n-γ spectrum for the first time as shown in Fig. 7. There is a clear peak at 247 keV in the spectrum, which is at the same energy as the $1/2^+_1 \rightarrow$ g.s.γ ray in ^{83}Ga [54]. This result shows that there is two-neutron branching in the decay of ^{85}Ga, which is consistent with the branching ratio obtained by the neutron detector, 1.6(2)%. The reported upper limit of the P_{2n} value by Miernik *et al.* was <0.1 %. The observed coincidence between two neutrons and the 247-keV γ ray supports that our P_{2n} value is more reliable. The discrepancy may be attributed to differences in detection energy thresholds for β particles.

TABLE II. List of γ rays observed in the decay of ^{84}Ga. I_γ is the number of γ rays emitted per 100 ^{84}Ga decays.

E_γ (keV)	I_γ (%)	$T_{1/2}$ (ms)	Decay channel
624.10(4)[a](38)[b]	6.4(2)[a](4)[b]	91(5)	β
1604.1(3)[a](4)[b]	0.69(18)[a](4)[b]		β
2877.7(3)[a](4)[b]	1.27(25)[a](8)[b]		β
3501.93(14)[a](38)[b]	5.3(3)[a](3)[b]	101(11)	β
247.58(20)[a](38)[b]	11.3(2)[a](7)[b]	88(2)	βn
798.97(35)[a](38)[b]	0.46(9)[a](3)[b]		βn
941.1(3)[a](4)[b]	1.01(11)[a](6)[b]		βn
1045.93(9)[a](38)[b]	7.4(3)[a](4)[b]	91(4)	βn
1204.3(5)[a](4)[b]	0.70(11)[a](4)[b]		βn
1239.38(21)[a](38)[b]	0.76(11)[a](5)[b]		βn
1794.80(19)[a](38)[b]	2.19(24)[a](13)[b]		βn[c]
1969.4(5)[a](4)[b]	0.78(13)[a](8)[b]	107(13)	βn[c]
2112.6(3)[a](4)[b]	0.33(8)[a](2)[b]	108(18)	βn
2910.7(4)[a](4)[b]	0.20(6)[a](2)[b]	85(20)	βn
217.3(5)[a](4)[b]	0.028(12)[a](2)[b]		$\beta 2n$[c]
1348.3(4)[a](4)[b]	0.47(9)[a](3)[b]	50(12)	$\beta 2n$

[a]Statistical errors.
[b]Systematic errors.
[c]Not assigned.

Levels of the daughter Ge nuclei constructed from this work are shown in Fig. 8. The levels in the ^{85}Ge nuclei are consistent with previous measurement [36,59]. Reference [59] assigned 773-keV peak to the decay of ^{84}As. We observed, however, a 78(12)-ms decay curve for this peak which supports the assignment of Ref. [36] as a transition in ^{85}Ge. As in Ref. [36] it assigned to a level at 773 keV since there was no coincidence observed with any other γ lines in ^{85}Ge. We observed 596-keV transition which was not reported in Ref. [36] but was observed in Ref. [59]. The 859-keV transition is assigned above the 1430-keV state since γ-γ coincidences are observed between the 806-keV and 624-keV transitions, as shown in Fig. 7. In addition, a new γ line at 1893 keV is observed and tentatively assigned as the decay from the new state at 3281 keV to the 1389-keV state because there is only one 1892-keV γ event recorded in coincidence with the 765-keV one, which is not sufficient to unambiguously assign the placement of the state. The list of γ-ray energy, half-lives, and intensities are summarized in Table III.

3. ^{86}Ga

The decay of the ^{86}Ga nucleus was previously reported by Miernik *et al.* [24]. The P_{xn} values from their work, $P_{1n} = 60(10)\%$ and $P_{2n} = 20(10)\%$, are consistent with our values, $P_{1n} = 60(3)\%$ and $P_{2n} = 14.7(14)\%$. β-γ spectra with neutron multiplicity gates are shown in Fig. 9 and the energies and intensities of the γ peaks are summarized in Table IV. We observed the 624-keV γ ray from the two-neutron decay channel that was reported in the previous study [24] but with two-neutron coincidences. We also observed γ rays from one-neutron decays reported in Ref. [24], in addition to the 472-

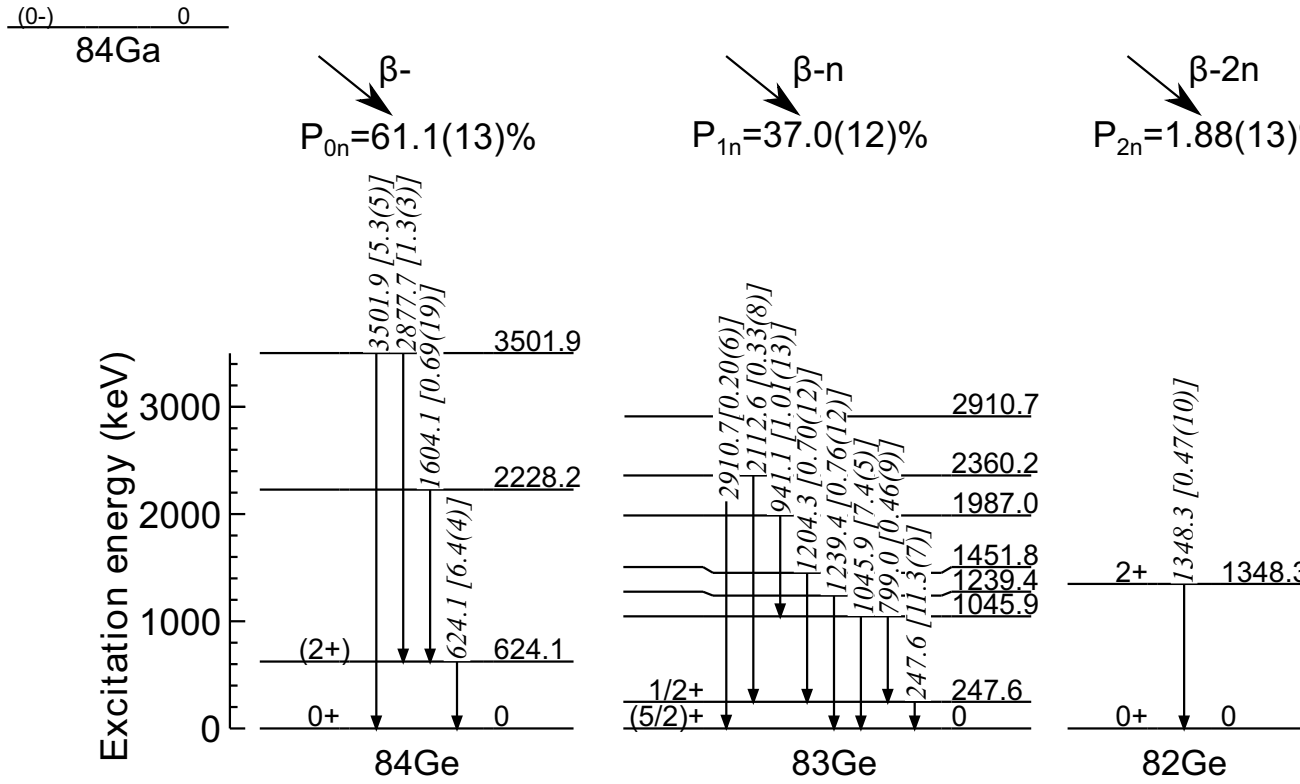

FIG. 6. Level scheme of $^{82-84}$Ge populated in the β decays of ^{84}Ga. Spin-parity assignments are from Refs. [56–58]. Intensities of the γ transitions in square brackets are given per 100 ^{84}Ga decays.

and 773-keV transitions which were previously known in the zero-neutron decay of ^{85}Ga [36]. A γ-ray peak at 1024 keV was observed in the zero-neutron emission channel. The half-life of the γ peak, 61(15) ms is consistent with the adopted decay half-life, 52(2) ms. Since there were no γ-γ coincidence events observed, it was tentatively assigned to a new state in ^{86}Ge at 1024 keV, a candidate for the second 2^+ state as reported by Ref. [56] at 1046(14). Levels of the daughter Ge nuclei observed in the decay of 86Ga are shown in Fig. 10.

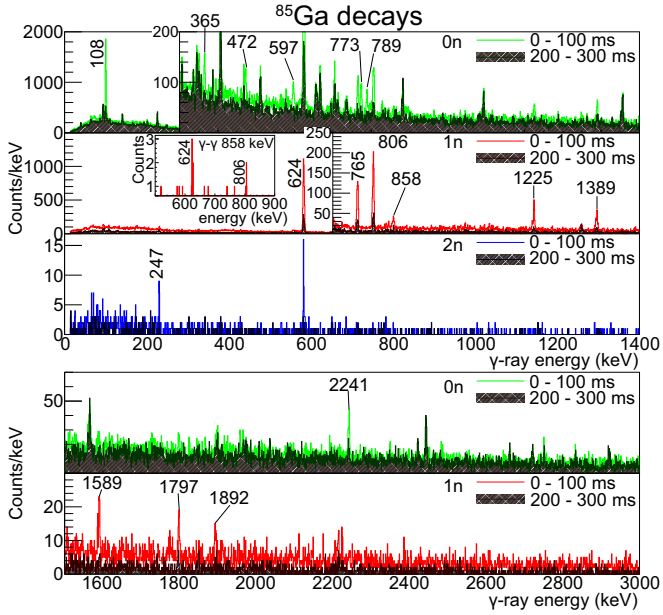

FIG. 7. γ-ray energy spectra of ^{85}Ga gated by neutron multiplicities. See the caption of Fig. 5 for details. A part of the γ-γ coincidence spectrum gated by the 858-keV peak is shown in the 1n spectrum in the upper panel.

4. ^{87}Ga

The decay of ^{87}Ga had not been measured before. The γ-ray spectra and the list of the peaks are shown in Fig. 11 and Table V, respectively. The $(2^+) \rightarrow 0^+$ transition in ^{86}Ge at 527 keV and the 108-keV transition in ^{85}Ga are observed in the decay of ^{87}Ga for the first time. The 786.1-keV peak in the 1n spectrum could be the 791(23)-keV transition from the (4_1^+) level in ^{86}Ga proposed by the Ref. [56] using in-flight γ-ray spectroscopy of the $(p, 2p)$ reaction.

C. Isomeric transition in ^{86}Ga

A delayed γ-ray peak was observed at 97.8(4) keV after the implantation of ^{86}Ga as shown in Fig. 12. The half-life of this isomeric state was observed to be 0.32(3) μs. The ground-state spin and parity (J^π) of the odd-odd $^{86}_{31}$Ga$_{55}$ nucleus is not known, and no excited states have ever been measured before. There is an isomer known in $^{92}_{37}$Rb$_{55}$ at 284.2 keV with a half-life of 54(3) ns [62]. This isomer decays by 142-keV $E2$ transition with $B(E2) = 7.2(4)$ W.u., which is typical for spherical nuclei around the $Z = 36$–40 region [62]. The new isomeric decay in ^{86}Ga has $B(E2) = 5.0(5)$ W.u. using the

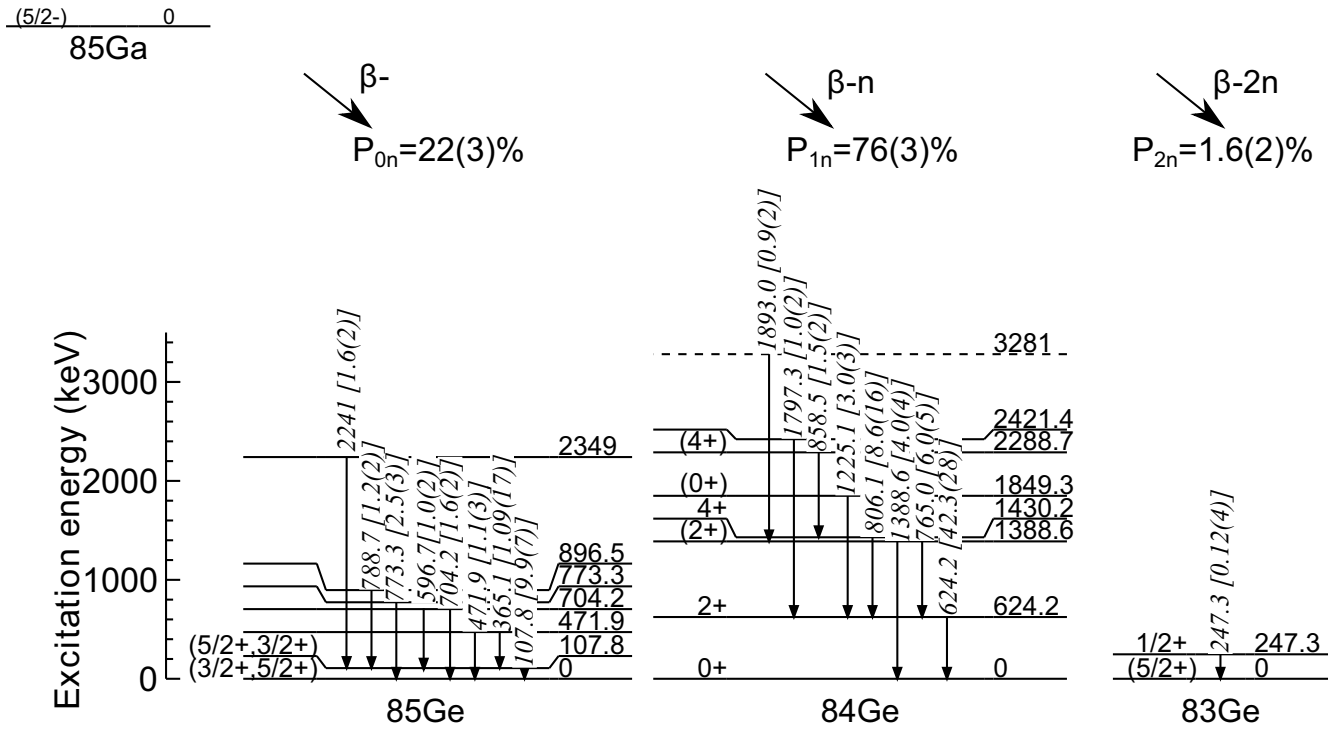

FIG. 8. Level scheme of $^{83-85}$Ge populated in the β decays of ^{85}Ga. Spin-parity assignments are from Refs. [56,57,60]. Intensities of the γ transitions in square brackets are given per 100 ^{85}Ga decays.

internal conversion coefficient from BRICC [63] assuming an $E2$ transition. This is a reasonable value for spherical nuclei as in the case of ^{92}Rb [62], and does not contrad various global calculations [64,65] predicting ^{86}Ga to be nearly spherical.

We performed shell-model calculations with the jj45pna interaction [66] using the KSHELL [67] code. It predicts the ground-state $J^\pi = 3^+$ for ^{86}Ga and a 5^+ state at 98 keV which decays by an $E2$ transition with 14.6 W.u. strength. On the other hand, NUSHELLX calculations predict two possibilities for low-lying iosmeric transitions: one with 7^+ and 5^+ pair and another with 2^- and 0^- pair with $B(E2)$ between 5 and 10 W.u. In both calculations, the configurations of the low-lying states are very fragmented between involved proton and neutron orbitals.

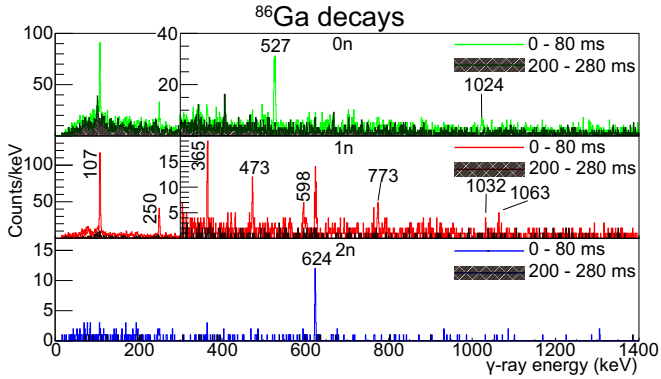

FIG. 9. γ-ray energy spectra of ^{86}Ga gated by neutron multiplicities.

TABLE III. List of γ rays observed in the decay of ^{85}Ga. I_γ is the number of γ rays emitted per 100 ^{85}Ga decays.

E_γ (keV)	I_γ (%)	$T_{1/2}$ (ms)	Decay channel
107.83(2)[a](38)[b]	9.9(3)[a](6)[b]	89(2)	β
365.15(16)[a](38)[b]	1.09(16)[a](7)[b]	107(16)	β
471.89(23)[a](38)[b]	1.10(27)[a](7)[b]		β
596.66(28)[a](38)[b]	1.04(17)[a](6)[b]	89(20)	β
704.20(17)[a](38)[b]	1.64(20)[a](10)[b]		β
773.30(17)[a](38)[b]	2.46(27)[a](15)[b]	84(11)	β
788.65(26)[a](38)[b]	1.21(22)[a](7)[b]	106(23)	β
2241.03(27)[a](38)[b]	1.65(21)[a](10)[b]	83(23)	β
624.18(27)[a](38)[b]	42.3(11)[a](25)[b]	92.5(17)	βn
765.02(9)[a](38)[b]	6.0(3)[a](7)[b]	89(7)	βn
806.06(8)[a](38)[b]	8.6(15)[a](5)[b]	92(4)	βn
858.5(4)[a](4)[b]	1.47(25)[a](17)[b]		βn
1225.08(14)[a](38)[b]	3.02(23)[a](18)[b]	96(6)	βn
1388.61(21)[a](38)[b]	4.03(30)[a](24)[b]	90(13)	βn
1588.9(4)[a](4)[b]	1.53(25)[a](17)[b]	100(13)	βn[c]
1797.3(4)[a](4)[b]	0.99(22)[a](11)[b]	85(12)	βn
1893.0(5)[a](4)[b]	0.91(25)[a](11)[b]	83(11)	βn
3359.3(5)[a](4)[b]	0.29(13)[a](3)[b]	75(27)	βn[c]
247.3(3)[a](4)[b]	0.12(4)[a](1)[b]		$\beta 2n$

[a]Statistical errors.
[b]Systematic errors.
[c]Not assigned.

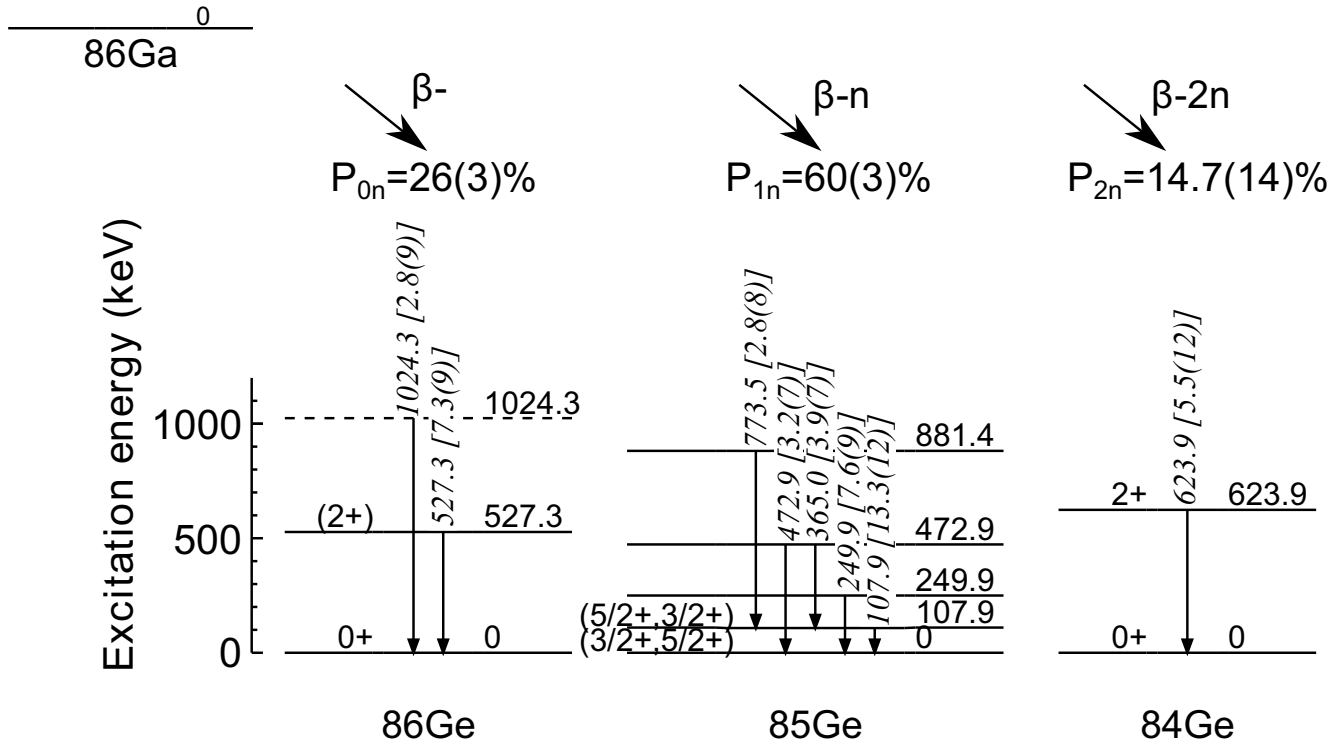

FIG. 10. Level scheme of $^{84-86}$Ge populated in the β decays of ^{86}Ga. Spin-parity assignments are from Refs. [56,60,61]. Intensities of the γ transitions in square brackets are given per 100 ^{86}Ga decays.

TABLE IV. List of γ rays observed in the decay of ^{86}Ga. I_γ is the number of γ rays emitted per 100 ^{86}Ga decays.

E_γ (keV)	I_γ (%)	$T_{1/2}$ (ms)	Decay channel
527.30(21)[a](38)[b]	7.3(8)[a](4)[b]	60(8)	β
1024.3(9)[a](4)[b]	2.8(9)[a](2)[b]		β
107.87(8)[a](38)[b]	13.3(9)[a](8)[b]	48(3)	βn
249.94(14)[a](38)[b]	7.6(7)[a](7)[b]	47(5)	βn
365.04(15)[a](38)[b]	3.9(6)[a](2)[b]	66(9)	βn
472.9(3)[a](4)[b]	3.2(7)[a](4)[b]	57(10)	βn
773.5(4)[a](4)[b]	2.8(8)[a](2)[b]		βn
623.89(18)[a](38)[b]	5.5(11)[a](5)[b]		$\beta 2n$

[a]Statistical errors.
[b]Systematic errors.

TABLE V. List of γ rays observed in the decay of ^{87}Ga. I_γ is the number of γ rays emitted per 100 ^{87}Ga decays.

E_γ (keV)	I_γ (%)	$T_{1/2}$ (ms)	Decay channel
1712.6(7)[a](4)[b]	6.9(34)[a](4)[b]		β[c]
2661.9(9)[a](4)[b]	6.5(43)[a](4)[b]		β[c]
178.2(6)[a](4)[b]	5.1(29)[a](6)[b]		βn[c]
527.2(3)[a](4)[b]	58(10)[a](6)[b]	27(8)	βn
786.1(3)[a](4)[b]	7.9(36)[a](9)[b]		βn
108.4(5)[a](4)[b]	10.9(45)[a](10)[b]		$\beta 2n$

[a]Statistical errors.
[b]Systematic errors.
[c]Not assigned.

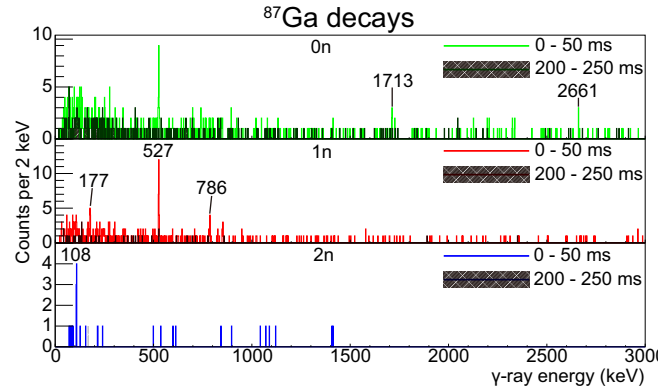

FIG. 11. γ-ray energy spectra of ^{87}Ga gated by neutron multiplicities.

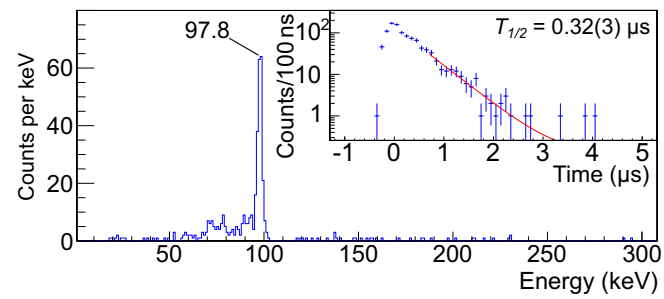

FIG. 12. Delayed γ-ray energy spectrum from 600 ns to 3 μs after implantation of the ^{86}Ga ion. The plot at the top right corner shows the decay curve of the 97.8 = keV γ line.

IV. DISCUSSION

The neutron energy spectra in the decay of ^{83,84}Ga were previously measured by Madurga *et al.* [34]. Observation of high-energy neutrons emitted after β decay was interpreted as a signature of the shell structure effects that dominate the β-decay process. In their work, a comparison between existing data and experiments was made for lifetimes and branching ratios, based on the determination of the details of the strength distribution, but no statistical model treatment was included to make predictions of P_{xn}.

As discussed in the previous paper [31], there is a discrepancy in the P_{1n} and P_{2n} values of ^{87}Ga between the experimental and the predicted values by Madurga *et al.* [34]. We applied the Hauser-Feshbach statistical model [38] to the shell-model calculation based on the work by Madurga [34], and the discrepancy was interpreted as one-neutron emission from two-neutron unbound states in the daughter nuclei. In this paper, we will describe more details of the shell model and the statistical model and will discuss the effect of level densities in daughter nuclei on the P_{xn} values by the statistical model calculation.

The model for the GT decay strength distribution for Ga isotopes [34] was based on a shell-model calculation for the β decay of Ga isotopes using the NUSHELLX code [68] with hybrid interactions and the truncation as previously described in [34,69,70]. In this model, the β-decay properties are dominated by the Gamow-Teller decay of the ^{78}Ni-core states, leaving the nucleus in the highly excited state because of the $N = 50$ shell gap. Good agreement between the $1n$ emission data predicted by the shell model and experimental data was achieved by choosing the 50% quenching factor on B(GT) as in Ref. [34] and kept it constant, which was deduced from the experimental neutron spectrum and adding the contribution from forbidden transitions.

An essential element of the description of this decay process in this framework is the contribution from the first forbidden transitions to the low excited states in Ge daughters. Despite their tiny matrix elements, their intensities are amplified by the phase space factor and result in a significant population of the neutron-bound states, thus suppressing the branching ratio of neutron emission channels. The inherent uncertainties of the B(GT) + FF models as well as decay energies and neutron separation energies require estimates of the expected lifetimes and P_{xn}. This was done by varying the scaling factor of the forbidden transition strength and shifting the B(GT) distribution. This analysis is required to find a possible scenario for the decay strength distribution, which will explain experimental data on $T_{1/2}$ and P_{0n} at the same time. We applied a 50% quenching factor on B(GT) as in Ref. [34] and kept it constant. The FF strength was constrained by P_{0n} and lifetimes. The concentration of B(GT) to highly excited, neutron-emitting states in Ge isotopes is the main reason why, given the large Q values, the nuclear lifetimes for Ga isotopes are relatively long. Figures 13(a) and 13(b) show the P_{0n} versus $T_{1/2}$ plots for ^{86,87}Ga with various offsets of the B(GT) distribution (GT shift) and scaling factors on the FF distribution (FF scale). Unlike P_{1n}/P_{2n}, P_{0n} is much less sensitive to the decay models since it almost only depends on

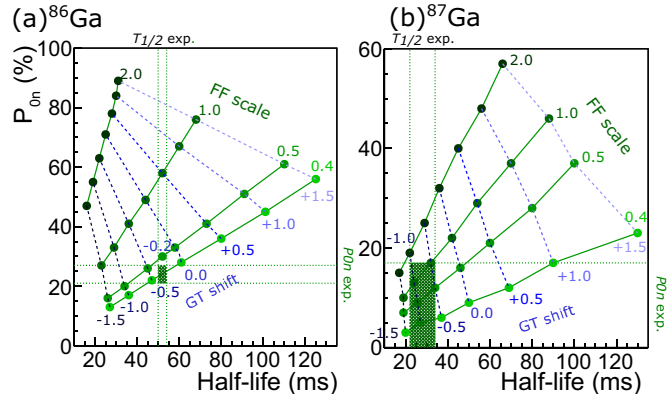

FIG. 13. P_{0n} versus $T_{1/2}$ plot for the shell-model calculations on ^{86,87}Ga. The hatched areas in the plots represent the experimental error bars on those values.

the β-decay intensity below the S_{1n} level, which is mostly the FF component. We selected the GT shift and FF scale values -0.2 and 0.4 for ^{86}Ga and -1.0 and 0.5 for ^{87}Ga.

The GT shift and FF scale values were also used in the calculations shown in the previous paper [31], which demonstrated that the statistical model correctly reproduces the dominant role of one-neutron emission from two-neutron unbound states.

As we calculated the branching ratios by the statistical model, we found that the decay patterns were sensitive to the level densities of the daughter nuclei. In the statistical model code by Kawano *et al.* [38], shell and pairing energies from the mass formula by Koura *et al.*, KTUY05, were applied to the Gilbert-Cameron formula [71] to generate phenomenological nuclear level densities [72]. The shell and pairing corrections were applied to the constant temperature level density formula,

$$\rho = \frac{1}{T}\exp\left(\frac{E - E_0}{T}\right), \tag{5}$$

as were the energy shift, E_0, and the systematic temperature, $T_{\rm syst}$, which are defined as follows:

$$E_0 = \Delta - \gamma_2 \delta w + T_{\rm syst} f(A),$$
$$T_{\rm syst} = \eta_1 A^{-\epsilon_1}\sqrt{1 - \gamma_1 \delta w}. \tag{6}$$

Δ and δw are the pairing energy and the shell correction, respectively, from the KTUY05 data. The smooth function of the mass number, $f(A)$, is defined in Ref. [72]. Also, a scaling factor, $f_{\rm tweak}$, was applied to the temperature:

$$T = T_{\rm syst}/f_{\rm tweak}. \tag{7}$$

The blue curve in Fig. 14 shows the default level density for ^{85}Ge, which is higher than the shell-model level densities shown as the red curve in the figure. To calculate the level densities, the NUSHELLX code with the jj45pna interaction was used to obtain as many states as possible. Due to our computational limit, levels up to ≈ 7 MeV were calculated for all the spins and parities. We fitted the shell-model level densities using Eq. (5), where δw, Δ, and $f_{\rm tweak}$ were free parameters. The level density function fitted for ^{85}Ge is shown

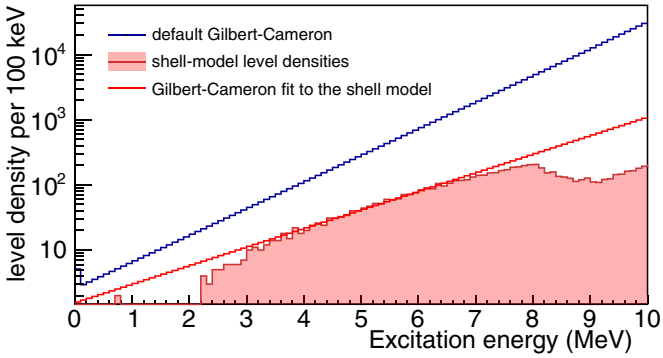

FIG. 14. Comparison of the default Gilbert-Cameron level densities in the statistical model and those from the shell-model calculation for ^{85}Ge.

as a red curve in Fig. 14. The fitting parameters for $^{83-86}$Ge are summarized in Table VI.

Statistical model calculations were performed on the decay of Ga isotopes with the default and the shell-model level densities of the daughter nuclei. Figure 15 shows the population of the excited states in the Ge daughters in the decay of ^{86}Ga. The β-decay feeding intensity in ^{86}Ge was based on the shell-model calculation. Only the GT part is considered in this plot because the FF part only affects P_{0n} but not $1n$-$2n$ competition. The excited states in ^{85,84}Ge are from the fitted level density but the low-lying levels are replaced with our experimental level schemes.

As shown in Fig. 16, P_{2n}/P_{1n} ratios changes by using different level densities in the statistical model calculations. The default level densities, which are higher than the shell-model ones, consistently predicted larger P_{2n} ratios for all four Ga isotopes. The higher level density above S_{1n} in the $1n$ daughter nucleus can result in a higher probability of emitting a second neutron. The experimental ratios agree better with the calculations with the shell-model level densities, which could mean the level densities of those Ge isotopes are lower than what was used in the statistical model with default parameters provided that we operate in the compound nucleus approximation.

The ground-state spin and parity (J^π) of the odd-odd ^{86}Ga nucleus is not known. We compared the P_{2n}/P_{1n} ratio and γ-ray branching ratio in the decay of ^{86}Ga by changing the input J^π of the statistical model calculation. As shown in Fig. 17, the statistical model predicts a clear trend of the γ-ray intensity ratio from the 4^+ and 2^+ states in the $2n$ decay channel, increasing when the initial spin of the parent nucleus

TABLE VI. List of parameters for the level density function.

	Default		Fit		
Nuclide	δw	Δ	δw	Δ	f_{tweak}
^{83}Ge	−3.71710	1.44894	4.88176	0.00000	0.147891
^{84}Ge	−3.07530	2.29824	−9.06038	4.03678	0.661307
^{85}Ge	−2.52280	1.44090	−7.41890	4.22327	0.786374
^{86}Ge	−1.83290	2.27325	−7.50608	4.20162	0.780135

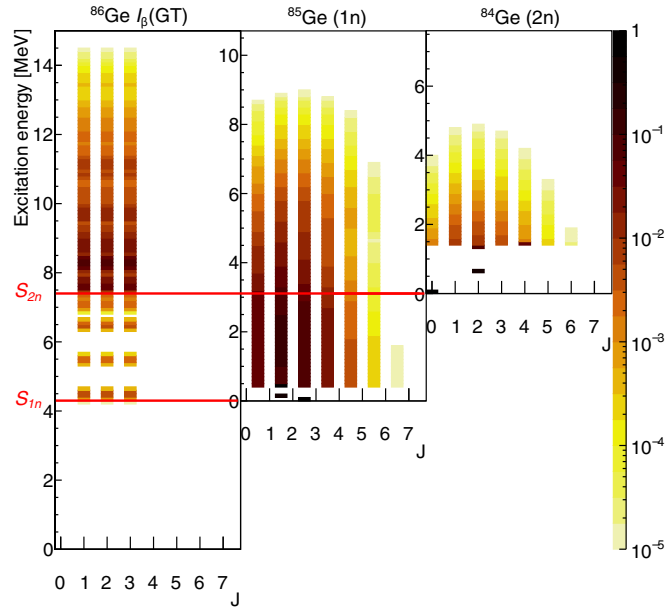

FIG. 15. Populations of the states excited by particle emission after the decay of ^{86}Ga simulated by the statistical model. $J^\pi = 2^-$ was assumed for the ground state of ^{86}Ga.

is increased. The P_{2n}/P_{1n} branching ratio, on the other hand, decreases for a higher J. In this work, the $4^+ \rightarrow 2^+$ γ line was not observed at 805 keV in the $2n$ gated spectrum (Fig. 9). The background level of the corresponding energy region was estimated to be ≈0.1 counts/keV by the log-likelihood fitting of the neighboring region around 805 keV. We set the minimum number of counts per keV to 3 as the detection limit of the 805-keV γ peak and deduced the upper limit of the $I_\gamma(4^+ \rightarrow 2^+)/I_\gamma(2^+ \rightarrow 0^+)$ ratio as 0.12, which is shown as a gray area in Fig 17(a). The probability of observing three counts within a 1-keV width bin by statistical fluctuation when the background rate is 0.1 is 1.5×10^{-4}, which is between 3σ and 4σ. In Fig. 17(b), the experimental P_{2n}/P_{1n} value is shown with an error of 1σ. In both plots, the lower spin scenarios ($J \leqslant 3$) agree with our experimental values.

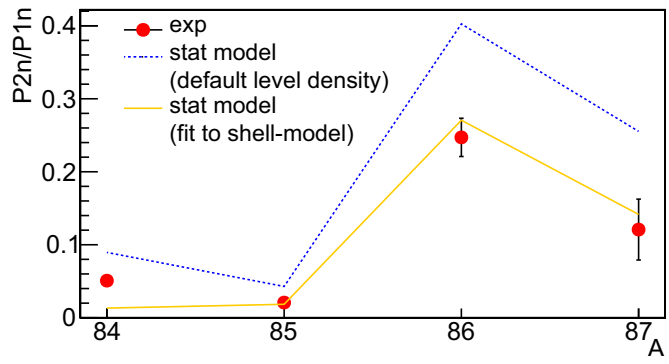

FIG. 16. P_{2n}/P_{1n} ratio in the decay of Ga isotopes. The red circle shows the experimental value while the blue-dashed and orange-solid lines show the shell-model predictions by using default and shell-model based parameters for the Gilbert-Cameron level densities, respectively.

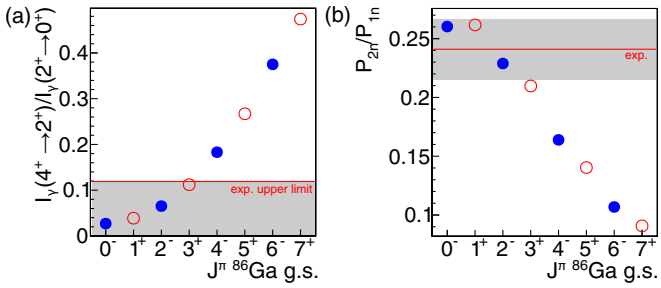

FIG. 17. Comparison of branching ratios calculated by the statistical model with the modified level densities with different assumptions on the unknown J^π of the parent nucleus in the decay of ^{86}Ga. Only odd spins for positive and even spins for negative parity states are presented for the sake of clarity. The blue circles and red open circles show negative and positive parity states, respectively. (a) γ-ray intensity ratio between $4^+ \rightarrow 2^+$ (805 keV) and $2^+ \rightarrow 0^+$ (624 keV) transitions of the ^{84}Ge nuclei in the $2n$ decay of ^{86}Ga. Since the 4^+ decay γ line was not observed, the experimental upper limit (see text for detail) is indicated by the red horizontal line. (b) P_{2n}/P_{1n} ratio. The red line shows the experimental value with a grey error band.

These results show the importance of the knowledge of the level densities and the ground-state spin of the parent nuclei for making reliable predictions of the multi-neutron emissions, and the requirement of further studies of neutron and γ-ray spectra to establish details of the emission process.

V. CONCLUSIONS

In summary, we performed β-γ-neutron analysis on $^{84–87}$Ga isotopes and performed statistical model calculations by using the experimental and shell-model levels in the daughter nuclei instead of the default level densities used in the code. We found that the multineutron emission ratio (P_{2n}/P_{1n}) is sensitive to the level density of the $A-1$ daughter nucleus, $^{83–86}$Ge, in this case. The statistical model calculation best reproduced the experimental P_{2n}/P_{1n} ratio when experimental levels plus shell-model level densities fitted by the Gilbert-Cameron formula are used as input. The neutron efficiencies of the BRIKEN array for each isotope were estimated by assuming the neutron spectra from the statistical model calculation to narrow down the systematic uncertainties in P_{xn} measurements. The P_{xn} values are updated from the ones reported in the previous paper [31] with a better estimation of neutron efficiencies. For ^{86}Ga decay, analysis of the neutron and γ branching ratios with the updated statistical model calculation suggests low spin for the ground state of the parent nucleus. These results show the importance of using correct level densities for the P_{xn} calculation and the necessity of neutron spectroscopy in addition to γ measurements of the multineutron emitters.

All of the relevant data of this study are available from the corresponding author upon reasonable request.

ACKNOWLEDGMENTS

This experiment was performed at the RI Beam Factory operated by RIKEN Nishina Center and CNS, University of Tokyo. This research was sponsored in part by the Office of Nuclear Physics, U.S. Department of Energy under Awards No. DE-FG02-96ER40983 (UTK), No. DE-AC05-00OR22725 (ORNL), and No. DE-SC0016988 (TTU) and by the National Nuclear Security Administration under the Stewardship Science Academic Alliances program through DOE Award No. DE-NA0002132. This work was supported by National Science Foundation under Grants No. PHY-1430152 (JINA Center for the Evolution of the Elements), No. PHY-1565546 (NSCL), and No. PHY-1714153 (Central Michigan University). This work was partially funded by the Polish National Science Center under Contracts No. UMO-2015/18/E/ST2/00217, No. 2020/39/B/ST2/02346, and No. 2017/01/X/ST2/01144. This work was also supported by JSPS KAKENHI (Grants No. 14F04808, No. 17H06090, No. 25247045, 20H05648, No. 22H04946, and No. 19340074), by the UK Science and Technology Facilities Council, by NKFIH (NN128072), by Spanish Ministerio de Economia y Competitividad grants (FPA2011-06419, FPA2011-28770-C03-03, FPA2014-52823-C2-1-P, FPA2014-52823-C2-2-P, SEV-2014-0398, IJCI-2014-19172), by Generarlitat Valenciana regional Grant No. PROMETEO/2019/007, by European Commission FP7/EURATOM Contract No. 605203, by the UK Science and Technology Facilities Council Grants No. ST/N00244X/1, No. ST//P004598/1, and No. ST/V001027/1, by the National Research Foundation (NRF) in South Korea (No. 2016K1A3A7A09005575 and No. 2015H1A2A1030275), and by the Natural Sciences and Engineering Research Council of Canada (NSERC) via the Discovery Grants No. SAPIN-2014-00028 and No. RGPAS 462257-2014. TRIUMF receives federal funding via a contribution agreement with the National Research Council of Canada. The author R.Y. acknowledges support from JSPS KAKENHI 22K14053. G.G.K. acknowledges support from the Janos Bolyai research fellowship of the Hungarian Academy of Sciences. M.W.-C. acknowledges support from the Polish NCN project Miniatura No. 2017/01/X/ST2/01144. M.P.-S. acknowledges support from Polish National Science Center Grants No. 2019/33/N/ST2/03023 and No. 2020/36/T/ST2/00547. T.K. carried out this work under the auspices of the National Nuclear Security Administration of the U.S. Department of Energy at Los Alamos National Laboratory under Contract No. 89233218CNA000001. A.A. Acknowledges partial support of the JSPS Invitational Fellowships for Research in Japan (ID: L1955).

[1] R. B. Roberts, R. C. Meyer, and P. Wang, Phys. Rev. **55**, 510 (1939).

[2] J. Liang, B. Singh, E. A. McCutchan, I. Dillmann, M. Birch, A. A. Sonzogni, X. Huang, M. Kang, J. Wang, G. Mukherjee,

K. Banerjee, D. Abriola, A. Algora, A. A. Chen, T. D. Johnson, and K. Miernik, Nucl. Data Sheets **168**, 1 (2020).
[3] P. Dimitriou, I. Dillmann, B. Singh, V. Piksaikin, K. Rykaczewski, J. Tain, A. Algora, K. Banerjee, I. Borzov, D. Cano-Ott, S. Chiba, M. Fallot, D. Foligno, R. Grzywacz, X. Huang, T. Marketin, F. Minato, G. Mukherjee, B. Rasco, A. Sonzogni *et al.*, Nucl. Data Sheets **173**, 144 (2021), Special Issue on Nuclear Reaction Data.
[4] R. Surman, M. Mumpower, and A. Aprahamian, JPS Conf. Proc. **6**, 010010 (2015).
[5] P. Möller, B. Pfeiffer, and K.-L. Kratz, Phys. Rev. C **67**, 055802 (2003).
[6] T. Marketin, L. Huther, and G. Martínez-Pinedo, Phys. Rev. C **93**, 025805 (2016).
[7] F. Minato, T. Marketin, and N. Paar, Phys. Rev. C **104**, 044321 (2021).
[8] A. Korgul, K. P. Rykaczewski, J. A. Winger, S. V. Ilyushkin, C. J. Gross, J. C. Batchelder, C. R. Bingham, I. N. Borzov, C. Goodin, R. Grzywacz, J. H. Hamilton, W. Królas, S. N. Liddick, C. Mazzocchi, C. Nelson, F. Nowacki, S. Padgett, A. Piechaczek, M. M. Rajabali, and D. Shapira *et al.*, Phys. Rev. C **86**, 024307 (2012).
[9] J. L. Tain, E. Valencia, A. Algora, J. Agramunt, B. Rubio, S. Rice, W. Gelletly, P. Regan, A. A. Zakari-Issoufou, M. Fallot, A. Porta, J. Rissanen, T. Eronen, J. Äystö, L. Batist, M. Bowry, V. M. Bui, R. Caballero-Folch, D. Cano-Ott, V. V. Elomaa *et al.*, Phys. Rev. Lett. **115**, 062502 (2015).
[10] B. C. Rasco, K. P. Rykaczewski, A. Fijałkowska, M. Karny, M. Wolińska-Cichocka, R. K. Grzywacz, C. J. Gross, D. W. Stracener, E. F. Zganjar, J. C. Blackmon, N. T. Brewer, K. C. Goetz, J. W. Johnson, C. U. Jost, J. H. Hamilton, K. Miernik, M. Madurga, D. Miller, S. Padgett, S. V. Paulauskas *et al.*, Phys. Rev. C **95**, 054328 (2017).
[11] A. Spyrou, S. N. Liddick, F. Naqvi, B. P. Crider, A. C. Dombos, D. L. Bleuel, B. A. Brown, A. Couture, L. Crespo Campo, M. Guttormsen, A. C. Larsen, R. Lewis, P. Möller, S. Mosby, M. R. Mumpower, G. Perdikakis, C. J. Prokop, T. Renstrøm, S. Siem, S. J. Quinn *et al.*, Phys. Rev. Lett. **117**, 142701 (2016).
[12] T. Kawano, P. Talou, I. Stetcu, and M. B. Chadwick, Nucl. Phys. A **913**, 51 (2013).
[13] M. R. Mumpower, T. Kawano, and P. Möller, Phys. Rev. C **94**, 064317 (2016).
[14] P. Möller, M. R. Mumpower, T. Kawano, and W. D. Myers, At. Data Nucl. Data Tables **125**, 1 (2019).
[15] R. E. Azuma, L. C. Carraz, P. G. Hansen, B. Jonson, K. L. Kratz, S. Mattsson, G. Nyman, H. Ohm, H. L. Ravn, A. Schroder, and W. Ziegert, Phys. Rev. Lett. **43**, 1652 (1979).
[16] J. Dufour, R. Delmoral, F. Hubert, D. Jean, M. Pravikoff, A. Fleury, A. Mueller, K.-H. Schmidt, K. Summerer, E. Hanelt, J. Frehaut, M. Meau, and G. Giraudet, Phys. Lett. B **206**, 195 (1988).
[17] K. Yoneda, N. Aoi, H. Iwasaki, H. Sakurai, H. Ogawa, T. Nakamura, W.-D. Schmidt-Ott, M. Schäfer, M. Notani, N. Fukuda, E. Ideguchi, T. Kishida, S. S. Yamamoto, and M. Ishihara, Phys. Rev. C **67**, 014316 (2003).
[18] V. Tripathi, S. L. Tabor, C. R. Hoffman, M. Wiedeking, A. Volya, P. F. Mantica, A. D. Davies, S. N. Liddick, W. F. Mueller, A. Stolz, B. E. Tomlin, T. Otsuka, and Y. Utsuno, Phys. Rev. C **73**, 054303 (2006).
[19] M. Langevin, C. Détraz, D. Guillemaud-Mueller, A. C. Mueller, C. Thibault, F. Touchard, and M. Epherre, Nucl. Phys. A **414**, 151 (1984).
[20] F. Perrot, F. Maréchal, C. Jollet, P. Dessagne, J. C. Angélique, G. Ban, P. Baumann, F. Benrachi, U. Bergmann, C. Borcea, A. Buta, J. Cederkall, S. Courtin, J. M. Daugas, L. M. Fraile, S. Grévy, A. Jokinen, F. R. Lecolley, E. Liénard, G. LeScornet *et al.*, Phys. Rev. C **74**, 014313 (2006).
[21] P. L. Reeder, R. A. Warner, T. R. Yeh, R. E. Chrien, R. L. Gill, M. Shmid, H. I. Liou, and M. L. Stelts, Phys. Rev. Lett. **47**, 483 (1981).
[22] B. Jonson, H. Gustafsson, P. Hansen, P. Hoff, P. Larsson, S. Mattsson, G. Nyman, H. Ravn, and D. Schardt, in *Proceedings of the 4th International Conference on Nuclei Far From Stability*, 7–13 June 1981, Helsingør, Denmark, CERN Report No. CERN-81-09 (CERN, Geneva, 1981), p. 265.
[23] R. Caballero-Folch, I. Dillmann, J. Agramunt, J. L. Taín, A. Algora, J. Äystö, F. Calviño, L. Canete, G. Cortès, C. Domingo-Pardo, T. Eronen, E. Ganioglu, W. Gelletly, D. Gorelov, V. Guadilla, J. Hakala, A. Jokinen, A. Kankainen, V. Kolhinen, J. Koponen *et al.*, Phys. Rev. C **98**, 034310 (2018).
[24] K. Miernik, K. P. Rykaczewski, C. J. Gross, R. Grzywacz, M. Madurga, D. Miller, J. C. Batchelder, I. N. Borzov, N. T. Brewer, C. Jost, A. Korgul, C. Mazzocchi, A. J. Mendez, Y. Liu, S. V. Paulauskas, D. W. Stracener, J. A. Winger, M. Wolińska-Cichocka, and E. F. Zganjar, Phys. Rev. Lett. **111**, 132502 (2013).
[25] B. Moon, C.-B. Moon, P.-A. Söderström, A. Odahara, R. Lozeva, B. Hong, F. Browne, H. S. Jung, P. Lee, C. S. Lee, A. Yagi, C. Yuan, S. Nishimura, P. Doornenbal, G. Lorusso, T. Sumikama, H. Watanabe, I. Kojouharov, T. Isobe, H. Baba *et al.*, Phys. Rev. C **95**, 044322 (2017).
[26] M. Piersa-Siłkowska, A. Korgul, J. Benito, L. M. Fraile, E. Adamska, A. N. Andreyev, R. Álvarez-Rodríguez, A. E. Barzakh, G. Benzoni, T. Berry, M. J. G. Borge, M. Carmona, K. Chrysalidis, J. G. Correia, C. Costache, J. G. Cubiss, T. Day Goodacre, H. De Witte, D. V. Fedorov, V. N. Fedosseev, S. G. Wilkins (IDS Collaboration) *et al.*, Phys. Rev. C **104**, 044328 (2021).
[27] J. Pereira, P. Hosmer, G. Lorusso, P. Santi, A. Couture, J. Daly, M. D. Santo, T. Elliot, J. Görres, C. Herlitzius, K. L. Kratz, L. O. Lamm, H. Y. Lee, F. Montes, M. Ouellette, E. Pellegrini, P. Reeder, H. Schatz, F. Schertz, L. Schnorrenberger *et al.*, Nucl. Instrum. Methods Phys. Res., Sect. A **618**, 275 (2010).
[28] R. Grzywacz, K. P. Rykaczewski, C. J. Gross, M. Madurga, K. Miernik, D. T. Miller, S. V. Paulauskas, S. W. Padgett, C. Rasco, M. Wolińska-Cichocka, and E. F. Zganjar, Acta Phys. Pol. B **45**, 217 (2014).
[29] M. B. Gómez-Hornillos, J. Rissanen, J. L. Taín, A. Algora, D. Cano-Ott, J. Agramunt, V. Gorlychev, R. Caballero, T. Martínez, L. Achouri, J. Äysto, G. Cortés, V. V. Elomaa, T. Eronen, A. García, J. Hakala, A. Jokinen, P. Karvonen, V. S. Kolhinen, I. Moore *et al.*, J. Phys.: Conf. Ser. **312**, 052008 (2011).
[30] A. Tarifeño-Saldivia, J. L. Tain, C. Domingo-Pardo, F. Calviño, G. Cortés, V. H. Phong, A. Riego, J. Agramunt, A. Algora, N. Brewer, R. Caballero-Folch, P. J. Coleman-Smith, T. Davinson, I. Dillmann, A. Estradé, C. J. Griffin, R. Grzywacz, L. J. Harkness-Brennan, G. G. Kiss, M. Kogimtzis *et al.*, J. Instrum. **12**, P04006 (2017).

[31] R. Yokoyama, R. Grzywacz, B. C. Rasco, N. Brewer, K. P. Rykaczewski, I. Dillmann, J. L. Tain, S. Nishimura, D. S. Ahn, A. Algora, J. M. Allmond, J. Agramunt, H. Baba, S. Bae, C. G. Bruno, R. Caballero-Folch, F. Calvino, P. J. Coleman-Smith, G. Cortes, T. Davinson *et al.*, Phys. Rev. C **100**, 031302 (2019).

[32] O. Hall, T. Davinson, A. Estrade, J. Liu, G. Lorusso, F. Montes, S. Nishimura, V. Phong, P. Woods, J. Agramunt, D. Ahn, A. Algora, J. Allmond, H. Baba, S. Bae, N. Brewer, C. Bruno, R. Caballero-Folch, F. Calviño, P. Coleman-Smith *et al.*, Phys. Lett. B **816**, 136266 (2021).

[33] V. H. Phong, S. Nishimura, G. Lorusso, T. Davinson, A. Estrade, O. Hall, T. Kawano, J. Liu, F. Montes, N. Nishimura, R. Grzywacz, K. P. Rykaczewski, J. Agramunt, D. S. Ahn, A. Algora, J. M. Allmond, H. Baba, S. Bae, N. T. Brewer, C. G. Bruno *et al.*, Phys. Rev. Lett. **129**, 172701 (2022).

[34] M. Madurga, S. V. Paulauskas, R. Grzywacz, D. Miller, D. W. Bardayan, J. C. Batchelder, N. T. Brewer, J. A. Cizewski, A. Fijałkowska, C. J. Gross, M. E. Howard, S. V. Ilyushkin, B. Manning, M. Matoš, A. J. Mendez, K. Miernik, S. W. Padgett, W. A. Peters, B. C. Rasco, A. Ratkiewicz *et al.*, Phys. Rev. Lett. **117**, 092502 (2016).

[35] J. A. Winger, S. V. Ilyushkin, K. P. Rykaczewski, C. J. Gross, J. C. Batchelder, C. Goodin, R. Grzywacz, J. H. Hamilton, A. Korgul, W. Królas, S. N. Liddick, C. Mazzocchi, S. Padgett, A. Piechaczek, M. M. Rajabali, D. Shapira, E. F. Zganjar, and I. N. Borzov, Phys. Rev. Lett. **102**, 142502 (2009).

[36] K. Miernik, K. P. Rykaczewski, R. Grzywacz, C. J. Gross, M. Madurga, D. Miller, D. W. Stracener, J. C. Batchelder, N. T. Brewer, A. Korgul, C. Mazzocchi, A. J. Mendez, II, Y. Liu, S. V. Paulauskas, J. A. Winger, M. Wolińska Cichocka, and E. F. Zganjar, Phys. Rev. C **97**, 054317 (2018).

[37] D. Verney, D. Testov, F. Ibrahim, Y. Penionzhkevich, B. Roussière, V. Smirnov, F. Didierjean, K. Flanagan, S. Franchoo, E. Kuznetsova, R. Li, B. Marsh, I. Matea, H. Pai, E. Sokol, I. Stefan, and D. Suzuki, Phys. Rev. C **95**, 054320 (2017).

[38] T. Kawano, P. Möller, and W. B. Wilson, Phys. Rev. C **78**, 054601 (2008).

[39] T. Kubo, Nucl. Instrum. Methods Phys. Res., Sect. B **204**, 97 (2003).

[40] H. Kumagai, A. Ozawa, N. Fukuda, K. Sümmerer, and I. Tanihata, Nucl. Instrum. Methods Phys. Res., Sect. A **470**, 562 (2001).

[41] K. Kimura, T. Izumikawa, R. Koyama, T. Ohnishi, T. Ohtsubo, a. Ozawa, W. Shinozaki, T. Suzuki, M. Takahashi, I. Tanihata, T. Yamaguchi, and Y. Yamaguchi, Nucl. Instrum. Methods Phys. Res., Sect. A **538**, 608 (2005).

[42] T. Ohnishi, T. Kubo, K. Kusaka, A. Yoshida, K. Yoshida, M. Ohtake, N. Fukuda, H. Takeda, D. Kameda, K. Tanaka, N. Inabe, Y. Yanagisawa, Y. Gono, H. Watanabe, H. Otsu, H. Baba, T. Ichihara, Y. Yamaguchi, M. Takechi, S. Nishimura *et al.*, J. Phys. Soc. Jpn. **79**, 073201 (2010).

[43] N. Fukuda, T. Kubo, T. Ohnishi, N. Inabe, H. Takeda, D. Kameda, and H. Suzuki, Nucl. Instrum. Methods Phys. Res., Sect. B **317**, 323 (2013).

[44] O. Hall, T. Davinson, C. Griffin, P. Woods, C. Appleton, C. Bruno, A. Estrade, D. Kahl, L. Sexton, I. Burrows, P. Coleman-Smith, M. Cordwell, A. Grant, M. Kogimtzis, M. Labiche, J. Lawson, I. Lazarus, P. Morall, V. Pucknell, J. Simpson *et al.*, Nucl. Instrum. Methods Phys. Res., Sect. A **1050**, 168166 (2023).

[45] S. Nishimura, G. Lorusso, Z. Xu, J. Wu, R. Gernh, H. S. Jung, Y. K. Kwon, Z. Li, K. Steiger, and H. Sakurai, RIKEN Accel. Prog. Rep. **46**, 182 (2013).

[46] R. Yokoyama, M. Singh, R. Grzywacz, A. Keeler, T. T. King, J. Agramunt, N. T. Brewer, S. Go, J. Heideman, J. Liu, S. Nishimura, P. Parkhurst, V. H. Phong, M. M. Rajabali, B. C. Rasco, K. P. Rykaczewski, D. W. Stracener, J. L. Tain, A. Tolosa-Delgado, K. Vaigneur *et al.*, Nucl. Instrum. Methods Phys. Res., Sect. A **937**, 93 (2019).

[47] E. Sahin, F. L. Bello Garrote, Y. Tsunoda, T. Otsuka, G. de Angelis, A. Görgen, M. Niikura, S. Nishimura, Z. Y. Xu, H. Baba, F. Browne, M.-C. Delattre, P. Doornenbal, S. Franchoo, G. Gey, K. Hadyńska-Klęk, T. Isobe, P. R. John, H. S. Jung, I. Kojouharov *et al.*, Phys. Rev. Lett. **118**, 242502 (2017).

[48] A. Tolosa-Delgado, J. Agramunt, J. L. Tain, A. Algora, C. Domingo-Pardo, A. I. Morales, B. Rubio, A. Tarifeño-Saldivia, F. Calviño, G. Cortes, N. T. Brewer, B. C. Rasco, K. P. Rykaczewski, D. W. Stracener, J. M. Allmond, R. Grzywacz, R. Yokoyama, M. Singh, T. King, M. Madurga *et al.*, Nucl. Instrum. Methods Phys. Res., Sect. A **925**, 133 (2019).

[49] B. C. Rasco, N. T. Brewer, R. Yokoyama, R. Grzywacz, K. P. Rykaczewski, A. Tolosa-Delgado, J. Agramunt, J. L. Tain, A. Algora, O. Hall, C. Griffin, T. Davinson, V. H. Phong, J. Liu, S. Nishimura, G. G. Kiss, N. Nepal, and A. Estrade, Nucl. Instrum. Methods Phys. Res., Sect. A **911**, 79 (2018).

[50] C. J. Gross, T. N. Ginter, D. Shapira, W. T. Milner, J. W. McConnell, A. N. James, J. W. Johnson, J. Mas, P. F. Mantica, R. L. Auble, J. J. Das, J. L. Blankenship, J. H. Hamilton, R. L. Robinson, Y. A. Akovali, C. Baktash, J. C. Batchelder, C. R. Bingham, M. J. Brinkman, H. K. Carter *et al.*, Nucl. Instrum. Methods Phys. Res., Sect. A **450**, 12 (2000).

[51] C. Mazzocchi, K. P. Rykaczewski, A. Korgul, R. Grzywacz, P. Baczyk, C. Bingham, N. T. Brewer, C. J. Gross, C. Jost, M. Karny, M. Madurga, A. J. Mendez, K. Miernik, D. Miller, S. Padgett, S. V. Paulauskas, D. W. Stracener, M. Wolińska-Cichocka, and I. N. Borzov, Phys. Rev. C **87**, 034315 (2013).

[52] A. Tolosa-Delgado, Ph.D. thesis, University of Valencia, 2020 (unpublished).

[53] K. Kolos, D. Verney, F. Ibrahim, F. Le Blanc, S. Franchoo, K. Sieja, F. Nowacki, C. Bonnin, M. Cheikh Mhamed, P. V. Cuong, F. Didierjean, G. Duchêne, S. Essabaa, G. Germogli, L. H. Khiem, C. Lau, I. Matea, M. Niikura, B. Roussière, I. Stefan, D. Testov, and J.-C. Thomas, Phys. Rev. C **88**, 047301 (2013).

[54] J. A. Winger, K. P. Rykaczewski, C. J. Gross, R. Grzywacz, J. C. Batchelder, C. Goodin, J. H. Hamilton, S. V. Ilyushkin, A. Korgul, W. Królas, S. N. Liddick, C. Mazzocchi, S. Padgett, A. Piechaczek, M. M. Rajabali, D. Shapira, E. F. Zganjar, and J. Dobaczewski, Phys. Rev. C **81**, 044303 (2010).

[55] I. Collaboration, Z. Phys. A **420**, 419 (1991).

[56] M. Lettmann, V. Werner, N. Pietralla, P. Doornenbal, A. Obertelli, T. R. Rodríguez, K. Sieja, G. Authelet, H. Baba, D. Calvet, F. Château, S. Chen, A. Corsi, A. Delbart, J.-M. Gheller, A. Giganon, A. Gillibert, V. Lapoux, T. Motobayashi, M. Niikura *et al.*, Phys. Rev. C **96**, 011301 (2017).

[57] E. McCutchan, Nucl. Data Sheets **125**, 201 (2015).

[58] J. Tuli and E. Browne, Nucl. Data Sheets **157**, 260 (2019).

[59] A. Korgul, K. P. Rykaczewski, R. Grzywacz, H. Sliwinska, J. C. Batchelder, C. Bingham, I. N. Borzov, N. Brewer, L. Cartegni, A. Fijalkowska, C. J. Gross, J. H. Hamilton, C. Jost, M. Karny, W. Krolas, S. Liu, C. Mazzocchi, M. Madurga, A. J. Mendez,

K. Miernik, D. Miller, S. Padgett, S. Paulauskas, D. Shapira, D. Stracener, K. Sieja, J. A. Winger, M. Wolinska-Cichocka, and E. F. Zganjar, Phys. Rev. C **88**, 044330 (2013).
[60] B. Singh and J. Chen, Nucl. Data Sheets **116**, 1 (2014).
[61] A. Negret and B. Singh, Nucl. Data Sheets **124**, 1 (2015).
[62] W. Urban, K. Sieja, G. S. Simpson, T. Soldner, T. Rząca-Urban, A. Złomaniec, I. Tsekhanovich, J. A. Dare, A. G. Smith, J. L. Durell, J. F. Smith, R. Orlandi, A. Scherillo, I. Ahmad, J. P. Greene, J. Jolie, and A. Linneman, Phys. Rev. C **85**, 014329 (2012).
[63] T. Kibédi, T. Burrows, M. Trzhaskovskaya, P. Davidson, and C. Nestor, Nucl. Instrum. Methods Phys. Res., Sect. A **589**, 202 (2008).
[64] S. Hilaire and M. Girod, Eur. Phys. J. A **33**, 237 (2007).
[65] P. Möller, A. J. Sierk, T. Ichikawa, and H. Sagawa, At. Data Nucl. Data Tables **109–110**, 1 (2016).
[66] B. A. Brown and W. D. M. Rae, in the package NUSHELL@MSU, 2014 (unpublished).
[67] N. Shimizu, T. Mizusaki, Y. Utsuno, and Y. Tsunoda, Comput. Phys. Commun. **244**, 372 (2019).
[68] B. A. Brown and W. D. M. Rae, Nucl. Data Sheets **120**, 115 (2014).
[69] C. Mazzocchi, A. Korgul, K. P. Rykaczewski, R. Grzywacz, P. Bączyk, C. R. Bingham, N. T. Brewer, C. J. Gross, C. Jost, M. Karny, M. Madurga, A. J. Mendez, K. Miernik, D. Miller, S. Padgett, S. V. Paulauskas, D. W. Stracener, and M. Wolińska-Cichocka, Acta Phys. Pol. B **46**, 713 (2015).
[70] M. F. Alshudifat, R. Grzywacz, M. Madurga, C. J. Gross, K. P. Rykaczewski, J. C. Batchelder, C. Bingham, I. N. Borzov, N. T. Brewer, L. Cartegni, A. Fijałkowska, J. H. Hamilton, J. K. Hwang, S. V. Ilyushkin, C. Jost, M. Karny, A. Korgul, W. Królas, S. H. Liu, C. Mazzocchi *et al.*, Phys. Rev. C **93**, 044325 (2016).
[71] A. Gilbert and A. G. W. Cameron, Can. J. Phys. **43**, 1446 (1965).
[72] T. Kawano, S. Chiba, and H. Koura, J. Nucl. Sci. Technol. **43**, 1 (2006).